Classical Rayleigh-Jeans Condensation of Light Waves: Observation and Thermodynamic Characterization

K. Baudin,[1] A. Fusaro,[1,2] K. Krupa,[1,3] J. Garnier,[4] S. Rica,[5] G. Millot,[1,6] and A. Picozzi[1]
[1]*Laboratoire Interdisciplinaire Carnot de Bourgogne, CNRS, Université Bourgogne Franche-Comté, 21078 Dijon, France*
[2]*CEA, DAM, DIF, F-91297 Arpajon Cedex, France*
[3]*Institute of Physical Chemistry, Polish Academy of Sciences, 01-224 Warsaw, Poland*
[4]*CMAP, CNRS, Ecole Polytechnique, Institut Polytechnique de Paris, 91128 Palaiseau Cedex, France*
[5]*Facultad de Ingeniería y Ciencias, Universidad Adolfo Ibáñez, Avda. Diagonal las Torres 2640, Peñalolén, 7910000, Santiago, Chile*
[6]*Institut Universitaire de France (IUF), 1 rue Descartes, 75005 Paris, France*

(Received 4 April 2020; revised 25 September 2020; accepted 16 November 2020; published 8 December 2020)

Theoretical studies on wave turbulence predict that a purely classical system of random waves can exhibit a process of condensation, which originates in the singularity of the Rayleigh-Jeans equilibrium distribution. We report the experimental observation of the transition to condensation of classical optical waves propagating in a multimode fiber, i.e., in a conservative Hamiltonian system without thermal heat bath. In contrast to conventional self-organization processes featured by the nonequilibrium formation of nonlinear coherent structures (solitons, vortices,…), here the self-organization originates in the equilibrium Rayleigh-Jeans statistics of classical waves. The experimental results show that the chemical potential reaches the lowest energy level at the transition to condensation, which leads to the macroscopic population of the fundamental mode of the optical fiber. The near-field and far-field measurements of the condensate fraction across the transition to condensation are in quantitative agreement with the Rayleigh-Jeans theory. The thermodynamics of classical wave condensation reveals that the heat capacity takes a constant value in the condensed state and tends to vanish above the transition in the normal state. Our experiments provide the first demonstration of a coherent phenomenon of self-organization that is exclusively driven by optical thermalization toward the Rayleigh-Jeans equilibrium.

DOI: 10.1103/PhysRevLett.125.244101

Several studies based on the wave turbulence theory [1–5] predict that nonlinear waves can exhibit a phenomenon of condensation [2,3,6–17]. This phenomenon of condensation of classical waves differs substantially from the quantum Bose-Einstein condensation (BEC) that has been observed in ultracold atoms and molecules [18], exciton polaritons [19], magnons [20], and photons [21,22]. Although the physics of BEC and classical condensation are different, the underlying mathematical origin is similar because of the common singular behavior (vanishing denominator) of the equilibrium Bose distribution for quantum particles and the equilibrium Rayleigh-Jeans (RJ) distribution for classical waves [3,7]. Here, we report the first observation of the RJ condensation of classical optical waves.

Various forms of condensation processes have been identified in optical cavity systems [19], which are inherently forced-dissipative systems operating far from thermal equilibrium [13,23–30]. On the other hand, equilibrium condensation mediated by the RJ distribution requires a (cavityless) free propagation of the optical beam through a conservative (Hamiltonian) evolution. However, as a consequence of the ultraviolet catastrophe inherent to classical waves, the RJ condensation is not defined for optical free propagation in a bulk medium. In this configuration, only a *nonequilibrium* transient process of condensation is experimentally accessible [15,17,31]. This problem can be circumvented by considering a waveguide configuration, whose finite number of modes introduces an effective frequency cutoff that regularizes the RJ ultraviolet catastrophe [13,32]. In this framework, a remarkable effect of spatial beam cleaning has been recently reported in multimode optical fibers (MMFs) [33,34]. Although recent works revealed that beam cleaning is characterized by a transfer of power toward the low-order modes of the MMF, the understanding of the underlying mechanism is still debated [32–43]. Yet despite experimental progress, there is still no clear-cut demonstration of the phenomenon of RJ condensation of optical waves.

From a broader perspective, wave condensation can be viewed as a self-organization process characterized by the formation of a *large scale coherent structure*, a universal behavior found in many fields of physics. As a general rule, the formation of a coherent structure (e.g., solitons, vortices, shock waves,…) requires a strong nonlinear interaction regime [2–14,44–49], as discussed in recent experiments in water tanks [50], vibrating elastic plates [51], BECs [49], or nonlinear optics [12,17,48,52]. More precisely, wave condensation is usually understood as an inverse turbulence cascade that increases the level of nonlinearity at large scales, up to a breaking point of the weak turbulence theory [3]. Such a nonlinear stage is well known in the focusing regime, where the (Benjamin-Feir) modulational instability leads to the generation of soliton-like structures (“soliton condensation”) [3,12,45–47]. This process is at the root of a variety of phenomena, e.g., optical filamentation [2,3], or soliton-mediated supercontinuum generation in optics [53] and hydrodynamics [54].

In contrast with this large variety of self-organization processes that occur far from thermal equilibrium and require a strong nonlinear interaction [2–10,12–14,44–52], we report in our experiments a different mechanism of spontaneous formation of a coherent structure (condensate) that is driven by the equilibrium RJ statistics in the weakly nonlinear regime. Condensation originates in the RJ distribution for the following reasons: (i) The transition takes place when the chemical potential reaches the fundamental mode eigenvalue, which leads to the macroscopic population of the fundamental mode of the MMF; (ii) the condensate fraction across the transition is in quantitative agreement with the RJ equilibrium theory (without adjustable parameters); (iii) the nonlinearity is perturbative with respect to linear propagation, even in the strongly condensed regime. Furthermore, our thermodynamic approach clarifies the different nature of the classical RJ transition with respect to the quantum BEC transition.

Aside from its fundamental importance, light cooling and condensation find natural applications to achieve an accurate control of the coherence properties of optical beams in high-power multimode fiber sources [55].

Experimental setup.—We study the spatial evolution of a speckle beam that propagates through a MMF featured by a parabolic-shaped index of refraction supporting $M \simeq 120$ modes. The 2D parabolic potential $V(\boldsymbol{r}) = q|\boldsymbol{r}|^2$ is truncated at $V_0 = qR^2$, where $R = 26\ \mu$m is the fiber radius and q a constant determined by the fiber characteristics. The eigenvalues are well approximated by the ideal harmonic potential $\beta_p = \beta_0(p_x + p_y + 1)$, where p labels the two integers (p_x, p_y) that specify a mode. The truncation of the potential $V(\boldsymbol{r}) \leq V_0$ and the corresponding finite number of modes M introduce an effective frequency cutoff in the far-field spectrum $k_c = \sqrt{2V_0/\beta_0}/r_0 \simeq 1.15\ \mu\text{m}^{-1}$, where r_0 is the radius of the fundamental mode of the MMF [56].

The source is a Nd:YAG laser ($\lambda_0 = 1.06\ \mu$m) delivering subnanosecond pulses that are passed through a diffuser before injection into the MMF. After propagation through a fiber length $L = 12$ m, the near-field (NF) and far-field (FF) intensities are recorded. The NF intensity $I_{\text{NF}}(\boldsymbol{r}) = |\psi|^2(\boldsymbol{r})$ provides the measurement of the power $N = \int I_{\text{NF}}(\boldsymbol{r})d\boldsymbol{r}$ and of the potential energy $E_{\text{pot}} = \int V(\boldsymbol{r})|\psi|^2(\boldsymbol{r})d\boldsymbol{r}$. The kinetic energy $E_{\text{kin}} = \alpha \int |\nabla\psi(\boldsymbol{r})|^2 d\boldsymbol{r}$ is retrieved from the FF intensity $I_{\text{FF}}(\boldsymbol{k}) = |\tilde{\psi}(\boldsymbol{k})|^2$, where $\alpha = 1/(2n_{\text{co}}k_0)$ with $k_0 = 2\pi/\lambda_0$ the laser wave number and n_{co} the refractive index $[\tilde{\psi}(\boldsymbol{k}) = (2\pi)^{-1} \int \psi(\boldsymbol{r}) \exp(i\boldsymbol{k}\cdot\boldsymbol{r})d\boldsymbol{r}$ being the Fourier transform]. This provides the linear contribution to the energy (Hamiltonian) $E = E_{\text{pot}} + E_{\text{kin}}$. Projecting on the basis of the fiber modes, the power and energy read $N = \sum_p n_p$, $E = \sum_p \beta_p n_p$, where n_p denotes the power in the mode p [11]. We have confirmed experimentally that both N and E are conserved during propagation in the MMF [56].

Weakly nonlinear regime.— The speckle beam that propagates through the MMF exhibits fluctuations that vary over a linear propagation length L_{lin} much smaller than the nonlinear length L_{nl}:

$$L_{\text{lin}} \sim \beta_0^{-1} \sim 0.2 \text{ mm} \ll L_{\text{nl}} = 1/(\gamma N) \sim 0.3 \text{ m}, \quad (1)$$

where γ is the nonlinear coefficient of the MMF. This is equivalent to $\lambda_c \ll \xi$, where $\xi = \sqrt{\alpha L_{\text{nl}}} \simeq 130\ \mu$m is the healing length, and λ_c the transverse correlation length of the speckle beam, which is typically smaller than the radius of the fundamental mode of the MMF, $\lambda_c \lesssim r_0 = \sqrt{2\alpha/\beta_0} \simeq 4.7\ \mu\text{m} \ll \xi$. Such a large separation between linear and nonlinear scales prevents a process of nonlinear self-organization. Then the *focusing* nature ($\gamma > 0$) of the fiber nonlinearity does not play any role: A spatial soliton cannot be generated since its width $\xi \gtrsim 130\ \mu$m would be much larger than the radius of the MMF ($R = 26\ \mu$m).

Rayleigh-Jeans thermalization.—In contrast with other experiments (e.g., Ref. [21]), here no thermal bath is present. As described by the wave turbulence theory and the numerical simulations, optical wave thermalization occurs through the propagation in the fiber as a consequence of the four-wave interaction underlying the Kerr nonlinearity [13,41]. This is a “closed” (Hamiltonian) system, where the conserved energy E is the control parameter of the transition to condensation. At equilibrium the modal populations follow the RJ distribution

$$n_p^{\text{eq}} = T/(\beta_p - \mu), \quad (2)$$

so that $N = T\sum_p(\beta_p - \mu)^{-1}$ and $E = T\sum_p \beta_p/(\beta_p - \mu)$. The solutions to these equations show that the pair (μ, T) is uniquely determined by the conserved quantities (N, E) [7,13,42] (T is in units of $\text{W}\cdot\text{m}^{-1}$ and it is not defined by a thermostat). At variance with previous experiments of spatial beam cleaning [33–36,40,43], here we study the transition to condensation by decreasing the energy E (“temperature”) while keeping constant the power N (“number of particles”)—E being varied owing to the diffuser before injection in the MMF [56].

We stress that RJ thermalization does not imply condensation: Here condensation occurs because the four-wave interaction is a $2 \leftrightarrow 2$ resonance with two conserved quantities (N, E). Systems like capillary waves, acoustic waves, Rossby planetary waves, or vibrating elastic plates do not conserve the "wave-action" N, so that $\mu = 0$ and condensation cannot take place: The fundamental mode cannot be macroscopically populated, i.e., $n_0^{\rm eq} \simeq n_p^{\rm eq}$ (for small p) whatever the energy.

Note that the stationary distribution describing light condensation in forced-dissipative lasers [27–30] resembles Eq. (2), provided one substitutes the β_p and the μ with the cavity losses and the gain, while T is fixed by a thermostat in Refs. [27–30]. Accordingly, the stationary distribution and its underlying mechanism of relaxation in Refs. [27–30] are fundamentally different from the RJ thermalization discussed here.

Considering the parabolic potential $V(\boldsymbol{r})$ and the corresponding invariance of the Hermite-Gauss modes (w_p) under Fourier transform, we have expressed the mean NF and FF intensities in equivalent forms. Splitting the condensate and the incoherent contributions $N = n_0^{\rm eq} + \sum_{p\neq 0} n_p^{\rm eq}$, we obtain [56]

$$I_{\rm NF}^{\rm cond}(r) = n_0^{\rm eq} r_0^2 w_0^2(r/r_0), \qquad I_{\rm FF}^{\rm cond}(k) = n_0^{\rm eq} r_0^{-2} w_0^2(r_0 k), \tag{3}$$

for the fundamental mode, and

$$I_{\rm NF}^{\rm inc}(r) = T \sum_{p\neq 0} r_0^{-2} w_p^2(\boldsymbol{r}/r_0)/(\beta_p - \mu), \tag{4}$$

$$I_{\rm FF}^{\rm inc}(k) = T \sum_{p\neq 0} r_0^{2} w_p^2(r_0 \boldsymbol{k})/(\beta_p - \mu), \tag{5}$$

for the incoherent contribution from the other modes. The total intensity is $I_{\rm NF}^{\rm eq}(r) = I_{\rm NF}^{\rm cond}(r) + I_{\rm NF}^{\rm inc}(r)$ (*idem* for the FF), with $N = \int I_{\rm NF}(\boldsymbol{r}) d\boldsymbol{r} = \int I_{\rm FF}(\boldsymbol{k}) d\boldsymbol{k}$, and $r = |\boldsymbol{r}|$, $k = |\boldsymbol{k}|$.

We performed averages from a total number of 2×1000 measurements of the NF and FF intensity distributions recorded for a fixed power $N = 7$ kW. We report in Figs. 1(a)–1(b) the NF and FF intensities for the same energy E (corresponding to $n_0^{\rm eq}/N \simeq 0.4$) that have been averaged over the realizations (blue lines). The experimental results are compared to the theoretical RJ intensity distributions (dashed red lines). The quantitative agreement in Figs. 1(a)–1(b) is obtained without any adjustable parameter: The experimentally measured values (E, N) determine a unique pair (μ, T), which in turn determines the intensity distributions $I_{\rm NF}^{\rm eq}(r)$ and $I_{\rm FF}^{\rm eq}(r)$ from Eqs. (3)–(5). As a result of the averaging procedure, the NF and FF representations are equivalent to each other [Eqs. (3)–(5)], as evidenced experimentally in Figs. 1(a)–1(b).

We compare the "output" intensity distributions recorded at 12 m with the "input" intensities recorded after 20 cm of propagation in the MMF ("initial conditions"). Figures 1(c)–1(d) report the NF and FF individual realizations of the input and output beams corresponding to

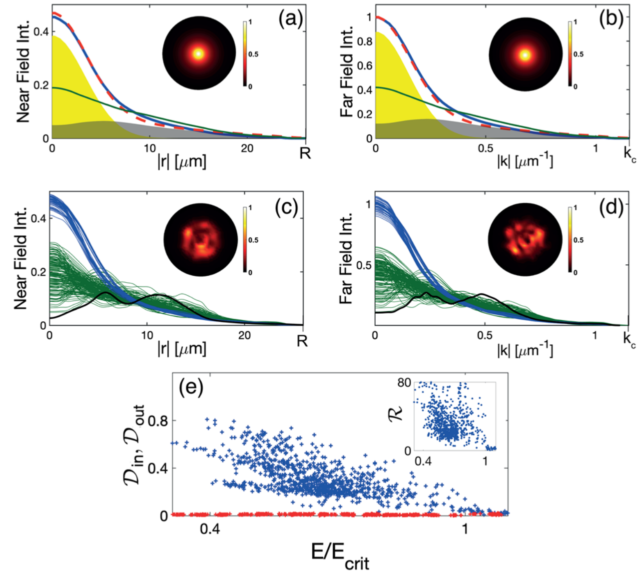

FIG. 1. Rayleigh-Jeans thermalization. Experimental profiles from the NF (a), and FF (b), intensity distributions recorded at the output of the MMF for the same energy $E/E_{\rm crit} \simeq 0.66$ ($n_0^{\rm eq}/N \simeq 0.4$) with an average over the realizations (blue lines). Theoretical RJ intensity distributions showing the condensate contribution from $p = 0$: $I_{\rm NF}^{\rm cond}(r)$, $I_{\rm FF}^{\rm cond}(k)$ [yellow region, from Eq. (3)], and the incoherent contribution from $p \neq 0$: $I_{\rm NF}^{\rm inc}(r)$, $I_{\rm FF}^{\rm inc}(k)$ [gray region, from Eqs. (4)–(5)], and their respective sums $I_{\rm NF}^{\rm eq}(r)$, $I_{\rm FF}^{\rm eq}(k)$ (dashed red lines)—note the quantitative agreement with the experiments (blue line) without adjustable parameters. The insets show the 2D intensity distributions averaged over the realizations. The green lines report the averaged intensity profiles recorded at the input of the MMF. (c)–(d) Individual realizations of the input (green) and output (blue) intensities corresponding to the average intensities in (a) and (b). The insets report the 2D intensity patterns corresponding to the black lines (same color bars for all insets). (e) Distance to the theoretical RJ intensity for all NF realizations of the input ($\mathcal{D}_{\rm in}$, blue) and output ($\mathcal{D}_{\rm out}$, red) intensities. The ratio $\mathcal{R} = \mathcal{D}_{\rm in}/\mathcal{D}_{\rm out} \gg 1$ shows the attraction to the RJ equilibrium (inset).

the averaged intensities of Figs. 1(a)–1(b): The input-to-output reduction of fluctuations enlightens the role of "statistical attractor" of the RJ distribution.

To characterize the RJ attraction process, we introduce a distance that measures the degree of similarity between the radial intensity distribution of a beam recorded experimentally and the theoretical RJ intensity: $\mathcal{D} = \sum_i [I_{\rm NF,exp}(r_i) - I_{\rm NF}^{\rm eq}(r_i)]^2 / \sum_i I_{\rm NF}^{\rm eq}(r_i)^2$, where $r = |\boldsymbol{r}|$ and r_i the corresponding spatial grid. The strong reduction of $\mathcal{D}$ from the input to the output beams confirms the thermalization to the RJ equilibrium; see Fig. 1(e) (the limited reduction of $\mathcal{D}$ for $E \gtrsim E_{\rm crit}$ is due to the polar-angle averaging procedure).

Rayleigh-Jeans condensation.—At variance with homogeneous condensation in a bulk medium [$V(\boldsymbol{r}) = 0$] [3,7], the presence of the parabolic potential reestablishes condensation in the "thermodynamic limit" in two dimensions. There exists a (nonvanishing) critical energy $E_{\rm crit}^* = NV_0/2$

such that $\mu = \beta_0$ [11,56]. At this critical point the denominator of the RJ distribution vanishes exactly [7] and the singularity is regularized by the macroscopic population of the fundamental mode [11,56]:

$$n_0^{\mathrm{eq}}/N = 1 - (E - E_0)/(E^*_{\mathrm{crit}} - E_0). \tag{6}$$

Then, n_0^{eq} vanishes at E^*_{crit}, and $n_0^{\mathrm{eq}}/N \to 1$ as E reaches the minimum $E_0 = N\beta_0$. This mechanism of RJ condensation is formally analogous to the quantum Bose-Einstein transition, which originates in the singularity of the Bose distribution when the chemical potential reaches the ground state energy [7,18].

Because of finite size effects, the experiment does not occur in the strict thermodynamic limit. The theory accounting for finite size effects gives $E_{\mathrm{crit}} = E_0[1 + (M-1)/\varrho]$, where $\varrho = \sum_{p\neq 0}(p_x + p_y)^{-1}$ [11,13,56]. Considering the experimental parameters we obtain $E^*_{\mathrm{crit}}/E_{\mathrm{crit}} \simeq 0.95$ [blue cross in Fig. 2(b)], so that our experiment is "close" to the thermodynamic limit.

In order to compare the theory with the experiments, we need to *extract* n_0^{eq} and μ from the experimental data. This requires a fitting procedure: Using the experimental intensities averaged over the realizations, we have retrieved (n_0^{eq}, μ) from the RJ intensity distributions [Eqs. (3)–(5)] by a least squares method [56]. For this purpose, the temperature T in Eqs. (4)–(5) has been expressed in terms of (n_0^{eq}, μ) by using $N = n_0^{\mathrm{eq}} + T\sum_{p\neq 0}(\beta_p - \mu)^{-1}$. In this way (n_0^{eq}, μ) can be extracted independently from either the NF or FF intensity distributions.

We report in Fig. 2(a) the chemical potential μ vs E: By decreasing E, μ increases and condensation occurs when $\mu \to \beta_0^-$ for $E = E_{\mathrm{crit}}$. Below the transition ($E \leq E_{\mathrm{crit}}$) the fundamental mode gets macroscopically populated, $n_0^{\mathrm{eq}} \gg n_{p\neq 0}^{\mathrm{eq}}$, see Fig. 2(b). The triangles report the experimental data retrieved from the least square method for the NF and FF intensity distributions. The red line reports the RJ theory accounting for finite size effects for the MMF used in the experiment; see Refs. [11,56]. The experimental results in Fig. 2 are in quantitative agreement with the RJ theory without adjustable parameters, i.e., β_0 and M are fixed by the MMF of the experiment [56]. Furthermore, the experimental results are close to the thermodynamic limit given by Eq. (6), see Fig. 2(b). As usual, finite size effects make the transition to condensation "smoother" [red line in Fig. 2(b)].

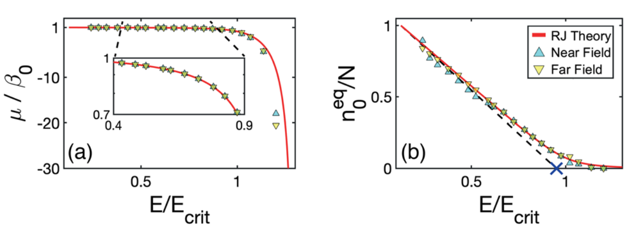

FIG. 2. Rayleigh-Jeans condensation. (a) Chemical potential vs energy: For $E \lesssim E_{\mathrm{crit}}$, $\mu \to \beta_0^-$, which leads to the macroscopic population of the fundamental mode, see n_0^{eq}/N vs E/E_{crit} (b). The blue (yellow) triangles report the experimental results from the NF (FF) intensity distributions (averaged over the realizations). The red lines report the RJ theory without using adjustable parameters. The dashed black line in (b) refers to the thermodynamic limit [Eq. (6)] and the blue cross denotes $E^*_{\mathrm{crit}}/E_{\mathrm{crit}} \simeq 0.95$: The experiment is "close" to the thermodynamic limit.

Thermodynamics of classical condensation.—We start from the *equilibrium* entropy $S^{\mathrm{eq}} = \sum_p \log(n_p^{\mathrm{eq}}) - M\log N$ that can be written $S^{\mathrm{eq}}(E) = -\sum_p \log[\beta_p - \mu(E)] - M\log\{\sum_p[\beta_p - \mu(E)]^{-1}\}$. Figure 3(a) reports S^{eq} vs E by using the experimental data $\mu(E)$ in Fig. 2(a). The heat capacity $C_V = (\partial E/\partial T)_{N,M}$ is an important quantity characterizing the transition to condensation [18]. In our experiment the transition is studied by varying E while holding N and M constant (M playing a role analogous to the system volume [32]). Using the energy-temperature relation E vs $T = (\partial E/\partial S^{\mathrm{eq}})_{N,M}$ in Fig. 3(b), we obtain [56]

$$C_V(E) = M - \frac{\{\sum_p[\beta_p - \mu(E)]^{-1}\}^2}{\sum_p[\beta_p - \mu(E)]^{-2}}. \tag{7}$$

Below the transition ($E < E_{\mathrm{crit}}$) we have $\mu \to \beta_0$. Then writing the energy in the form $E = TM + \beta_0 N$ gives $C_V = M$, as expected from the theorem of energy equipartition, see Figs. 3(c)–3(d).

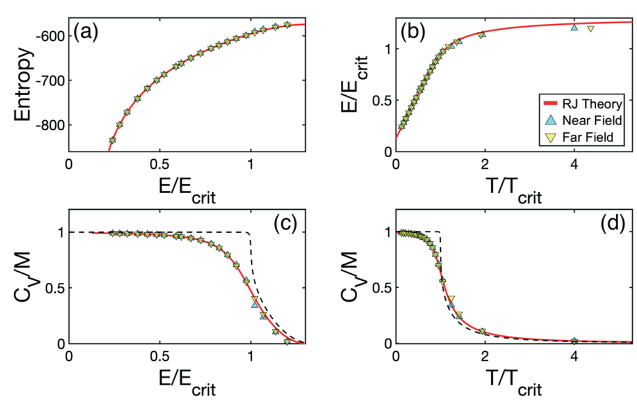

FIG. 3. Thermodynamics of classical condensation. (a) Entropy S^{eq} vs E/E_{crit}; (b) E/E_{crit} vs T/T_{crit}. Heat capacity C_V/M vs E/E_{crit} (c), and vs T/T_{crit} (d). The blue (yellow) triangles report the experimental results from the NF (FF) intensity distributions (averaged over the realizations). The solid red lines report the RJ theory without adjustable parameters ($M = 120$ modes). For $E < E_{\mathrm{crit}}$ (or $T < T_{\mathrm{crit}}$) the system exhibits energy equipartition among the modes and $C_V/M \to 1$, whereas for $E > E_{\mathrm{crit}}$ (or $T > T_{\mathrm{crit}}$) the equipartition of power among the modes entails $C_V \to 0$ (dashed-black lines are for $M = 500\,500$).

Far above the BEC transition a quantum gas behaves as a classical gas featured by a constant heat capacity $C_V(T) = \text{const}$ [18]. At variance with a classical gas, we observe in our classical wave system that $C_V \to 0$ for $E > E_{\rm crit}$ (or $T > T_{\rm crit} = N\beta_0/\varrho$), see Figs. 3(c)–3(d). Actually, the equilibrium properties of waves are of a different nature than those of a gas: Above the transition the equilibrium state no longer exhibits energy equipartition, but instead an equipartition of the power among the modes, viz $n_p^{\rm eq} \sim T/(-\mu)$ for $-\mu \gg \beta_p$. This is the most disordered equilibrium state with $S_{\rm max}^{\rm eq} = -M \log M$ for $E = \frac{2}{3} N V_0$ and $1/T = (\partial S/\partial E)_{N,M} \to 0$. This means that the equilibrium is *not constrained by the conservation of the energy E* (the Lagrange multiplier $1/T$ is zero), but solely by the conservation of N, which merely explains the modal power equipartition [60]. Accordingly, a variation of T does not affect E, which entails $C_V \to 0$. Approaching the thermodynamic limit, C_V exhibits a cusp featured by an infinite derivative at $E = E_{\rm crit}$ (or $T = T_{\rm crit}$); see Figs. 3(c)–3(d).

Conclusion.—We have reported the first observation of the equilibrium condensation of classical optical waves in quantitative agreement with the RJ theory. Far above the transition, the field exhibits an equipartition of power among the modes and a vanishing heat capacity $[C_V(T) \to 0]$. Below the transition ($E < E_{\rm crit}$), the fundamental mode is macroscopically populated and the constant heat capacity reflects an energy equipartition among the uncondensed modes.

Our experiments in MMFs pave the way for a thermodynamic control of light coherence [32,61]. For instance, a thermalized speckle beam in the normal state can be adiabatically cooled to the condensed state owing to a potential sink in a manufactured MMF, in analogy with the adiabatic formation of quantum BECs [18].

The authors are grateful to I. Carusotto, C. Michel, R. Kaiser, P. Béjot, P. Aschieri, V. Doya, A. Tonello, V. Couderc, and A. Barthélemy for fruitful discussions. We acknowledge financial support from the French ANR under Grant No. ANR-19-CE46-0007 (project ICCI), iXcore research foundation, EIPHI Graduate School (Contract No. ANR-17-EURE-0002), French program “Investissement d’Avenir,” Project No. ISITE-BFC-299 (ANR-15 IDEX-0003); H2020 Marie Sklodowska-Curie Actions (MSCA-COFUND) (MULTIPLY Project No. 713694). S. R. thanks FONDECYT Grant (ANID-Chile) No. 1181382.

[1] V. E. Zakharov, V. S. L’vov, and G. Falkovich, *Kolmogorov Spectra of Turbulence I* (Springer, Berlin, 1992).
[2] A. C. Newell, S. Nazarenko, and L. Biven, Wave turbulence and intermittency, Physica (Amsterdam) **152D**, 520 (2001).
[3] S. Nazarenko, *Wave Turbulence*, Lectures Notes in Physics (Springer, New York, 2011).
[4] A. C. Newell and B. Rumpf, Wave turbulence, Annu. Rev. Fluid Mech. **43**, 59 (2011).
[5] *Advances in Wave Turbulence*, World Scientific Series on Nonlinear Science Series A Vol. 83, edited by V. I. Shrira and S. Nazarenko (World Scientific, Singapore, 2013).
[6] V. E. Zakharov and S. V. Nazarenko, Dynamics of the Bose-Einstein condensation, Physica (Amsterdam) **201D**, 203 (2005).
[7] C. Connaughton, C. Josserand, A. Picozzi, Y. Pomeau, and S. Rica, Condensation of Classical Nonlinear Waves, Phys. Rev. Lett. **95**, 263901 (2005).
[8] S. Nazarenko and M. Onorato, Wave turbulence and vortices in Bose-Einstein condensation, Physica (Amsterdam) **219D**, 1 (2006).
[9] N. G. Berloff and A. J. Youd, Dissipative Dynamics of Superfluid Vortices at Nonzero Temperatures, Phys. Rev. Lett. **99**, 145301 (2007).
[10] G. Düring, A. Picozzi, and S. Rica, Breakdown of weak-turbulence and nonlinear wave condensation, Physica (Amsterdam) **238D**, 1524 (2009).
[11] P. Aschieri, J. Garnier, C. Michel, V. Doya, and A. Picozzi, Condensation and thermalization of classsical optical waves in a waveguide, Phys. Rev. A **83**, 033838 (2011).
[12] J. Laurie, U. Bortolozzo, S. Nazarenko, and S. Residori, One-dimensional optical wave turbulence: Experiment and theory, Phys. Rep. **514**, 121 (2012).
[13] A. Picozzi, J. Garnier, T. Hansson, P. Suret, S. Randoux, G. Millot, and D. N. Christodoulides, Optical wave turbulence: Toward a unified nonequilibrium thermodynamic formulation of statistical nonlinear optics, Phys. Rep. **542**, 1 (2014).
[14] S. Nazarenko, M. Onorato, and D. Proment, Bose-Einstein condensation and Berezinskii-Kosterlitz-Thouless transition in the two-dimensional nonlinear Schrödinger model, Phys. Rev. A **90**, 013624 (2014).
[15] C. Sun, S. Jia, C. Barsi, S. Rica, A. Picozzi, and J. Fleischer, Observation of the kinetic condensation of classical waves, Nat. Phys. **8**, 470 (2012).
[16] A. Rückriegel and P. Kopietz, Rayleigh-Jeans Condensation of Pumped Magnons in Thin-Film Ferromagnets, Phys. Rev. Lett. **115**, 157203 (2015).
[17] N. Santic, A. Fusaro, S. Salem, J. Garnier, A. Picozzi, and R. Kaiser, Nonequilibrium Precondensation of Classical Waves in Two Dimensions Propagating through Atomic Vapors, Phys. Rev. Lett. **120**, 055301 (2018).
[18] S. Pitaevskii and L. Stringari, *Bose-Einstein Condensation* (Oxford Science Publications, New York, 2003).
[19] I. Carusotto and C. Ciuti, Quantum fluids of light, Rev. Mod. Phys. **85**, 299 (2013).
[20] S. O. Demokritov, V. E. Demidov, O. Dzyapko, G. A. Melkov, A. A. Serga, B. Hillebrands, and A. N. Slavin, Bose-Einstein condensation of quasi-equilibrium magnons at room temperature under pumping, Nature (London) **443**, 430 (2006).
[21] J. Klaers, J. Schmitt, F. Vewinger, and M. Weitz, Bose-Einstein condensation of photons in an optical microcavity, Nature (London) **468**, 545 (2010).

[22] R. Weill, A. Bekker, B. Levit, and B. Fischer, Bose-Einstein condensation of photons in an erbium-ytterbium co-doped fiber cavity, Nat. Commun. **10**, 747 (2019).

[23] C. Conti, M. Leonetti, A. Fratalocchi, L. Angelani, and G. Ruocco, Condensation in Disordered Lasers: Theory, $3d+1$ Simulations, and Experiments, Phys. Rev. Lett. **101**, 143901 (2008).

[24] N. G. Berloff and J. Keeling, Universality in modelling non-equilibrium polariton condensates, in *Physics of Quantum Fluids*, edited by A. Bramati and M. Modugno, Springer Series in Solid-State Sciences Vol. 177 (Springer, Berlin, Heidelberg, 2013).

[25] E. Turitsyna, S. Smirnov, S. Sugavanam, N. Tarasov, X. Shu, S. Babin, E. Podivilov, D. Churkin, G. Falkovich, and S. Turitsyn, The laminar-turbulent transition in a fibre laser, Nat. Photonics **7**, 783 (2013).

[26] D. Churkin, I. Kolokolov, E. Podivilov, I. Vatnik, S. Vergeles, I. Terekhov, V. Lebedev, G. Falkovich, M. Nikulin, S. Babin, and S. Turitsyn, Wave kinetics of a random fibre laser, Nat. Commun. **6**, 6214 (2015).

[27] R. Weill, B. Fischer, and O. Gat, Light-Mode Condensation in Actively-Mode-Locked Lasers, Phys. Rev. Lett. **104**, 173901 (2010).

[28] B. Fischer and R. Weill, When does single-mode lasing become a condensation phenomenon? Opt. Express **20**, 26704 (2012).

[29] G. Oren, A. Bekker, and B. Fischer, Classical condensation of light pulses in a loss trap in a laser cavity, Optica **1**, 145 (2014).

[30] G. Oren, A. Bekker, and B. Fischer, CW laser light condensation, Opt. Express **24**, 6553 (2016).

[31] A. Chiocchetta, P. E. Larré, and I. Carusotto, Thermalization and Bose-Einstein condensation of quantum light in bulk nonlinear media, Europhys. Lett. **115**, 24002 (2016).

[32] F. O. Wu, A. U. Hassan, and D. N. Christodoulides, Thermodynamic theory of highly multimoded nonlinear optical systems, Nat. Photonics **13**, 776 (2019).

[33] L. G. Wright, Z. Liu, D. A. Nolan, M.-J. Li, D. N. Christodoulides, and F. W. Wise, Self-organized instability in graded-index multimode fibres, Nat. Photonics **10**, 771 (2016).

[34] K. Krupa, A. Tonello, B. M. Shalaby, M. Fabert, A. Barthélémy, G. Millot, S. Wabnitz, and V. Couderc, Spatial beam self-cleaning in multimode fibres, Nat. Photonics **11**, 237 (2017).

[35] K. Krupa, A. Tonello, A. Barthélémy, V. Couderc, B. M. Shalaby, A. Bendahmane, G. Millot, and S. Wabnitz, Observation of Geometric Parametric Instability Induced by the Periodic Spatial Self-Imaging of Multimode Waves, Phys. Rev. Lett. **116**, 183901 (2016).

[36] Z. Liu, L. G. Wright, D. N. Christodoulides, and F. W. Wise, Kerr self-cleaning of femtosecond-pulsed beams in graded-index multimode fiber, Opt. Lett. **41**, 3675 (2016).

[37] J. Laegsgaard, Spatial beam cleanup by pure Kerr processes in multimode fibers, Opt. Lett. **43**, 2700 (2018).

[38] C. Mas Arabi, A. Kudlinski, A. Mussot, and M. Conforti, Geometric parametric instability in periodically modulated graded-index multimode fibers, Phys. Rev. A **97**, 023803 (2018).

[39] A. Fusaro, J. Garnier, K. Krupa, G. Millot, and A. Picozzi, Dramatic Acceleration of Wave Condensation Mediated by Disorder in Multimode Fibers, Phys. Rev. Lett. **122**, 123902 (2019).

[40] E. Podivilov, D. Kharenko, V. Gonta, K. Krupa, O. S. Sidelnikov, S. Turitsyn, M. P. Fedoruk, S. A. Babin, and S. Wabnitz, Hydrodynamic 2D Turbulence and Spatial Beam Condensation in Multimode Optical Fibers, Phys. Rev. Lett. **122**, 103902 (2019).

[41] J. Garnier, A. Fusaro, K. Baudin, C. Michel, K. Krupa, G. Millot, and A. Picozzi, Wave condensation with weak disorder versus beam self-cleaning in multimode fibers, Phys. Rev. A **100**, 053835 (2019).

[42] M. Parto, F. Wu, P. Jung, K. Makris, and D. Christodoulides, Thermodynamic conditions governing the optical temperature and chemical potential in nonlinear highly multimoded photonic systems, Opt. Lett. **44**, 3936 (2019).

[43] K. Krupa, A. Tonello, A. Barthélémy, T. Mansuryan, V. Couderc, G. Millot, P. Grelu, D. Modotto, S. A. Babin, and S. Wabnitz, Multimode nonlinear fiber optics, a spatiotemporal avenue, APL Photonics **4**, 110901 (2019).

[44] P. A. E. M. Janssen, *The Interaction of Ocean Waves and Wind* (Cambridge University Press, Cambridge, 2004).

[45] B. Rumpf and A. C. Newell, Coherent Structures and Entropy in Constrained, Modulationally Unstable, Nonintegrable Systems, Phys. Rev. Lett. **87**, 054102 (2001).

[46] V. Zakharov, F. Dias, and A. Pushkarev, One-dimensional wave turbulence, Phys. Rep. **398**, 1 (2004).

[47] B. Rumpf, A. C. Newell, and V. E. Zakharov, Turbulent Transfer of Energy by Radiating Pulses, Phys. Rev. Lett. **103**, 074502 (2009).

[48] G. Xu, D. Vocke, D. Faccio, J. Garnier, T. Rogers, S. Trillo, and A. Picozzi, From coherent shocklets to giant collective incoherent shock waves in nonlocal turbulent flows, Nat. Commun. **6**, 8131 (2015).

[49] M. C. Tsatsos, P. E. S. Tavares, A. Cidrim, A. R. Fritsch, M. A. Caracanhas, F. E. A. dos Santos, C. F. Barenghi, and V. S. Bagnato, Quantum turbulence in trapped atomic Bose-Einstein condensates, Phys. Rep. **622**, 1 (2016).

[50] R. Hassaini and N. Mordant, Transition from weak wave turbulence to soliton gas, Phys. Rev. Fluids **2**, 094803 (2017).

[51] B. Miquel, A. Alexakis, C. Josserand, and N. Mordant, Transition from Wave Turbulence to Dynamical Crumpling in Vibrated Elastic Plates, Phys. Rev. Lett. **111**, 054302 (2013).

[52] D. Pierangeli, F. Di Mei, G. Di Domenico, A. J. Agranat, C. Conti, and E. DelRe, Turbulent Transitions in Optical Wave Propagation, Phys. Rev. Lett. **117**, 183902 (2016).

[53] J. M. Dudley, G. Genty, and S. Coen, Supercontinuum generation in photonic crystal fiber, Rev. Mod. Phys. **78**, 1135 (2006).

[54] A. Chabchoub, N. Hoffmann, M. Onorato, G. Genty, J. M. Dudley, and N. Akhmediev, Hydrodynamic Supercontinuum, Phys. Rev. Lett. **111**, 054104 (2013).

[55] L. G. Wright, D. N. Christodoulides, and F. W. Wise, Spatiotemporal mode-locking in multimode fiber lasers, Science **358**, 94 (2017).

[56] See Supplemental Material at http://link.aps.org/supplemental/10.1103/PhysRevLett.125.244101 for details

about the experimental procedures (fitting of n_0^{eq} and μ; conservation of N and E through propagation), and the detailed derivation of Eqs. (3)–(7), which includes Refs. [57–59]. It also summarizes the theory of RJ condensation with a trapping potential (red lines in Fig. 2) reported in Ref. [11].

[57] D. E. B. Flaes, J. Stopka, S. Turtaev, J. F. de Boer, T. Tyc, and T. Čižmár, Robustness of Light-Transport Processes to Bending Deformations in Graded-Index Multimode Waveguides, Phys. Rev. Lett. **120**, 233901 (2018).

[58] D. Marcuse, D. Gloge, and E. A. J. Marcatili, Guiding properties of fibers, in *Optical Fiber Telecommunications*, edited by S. E. Miller and A. G. Chynoweth (Academic Press, New York, 1979).

[59] P. Suret and S. Randoux, Far field measurement in the focal plane of a lens: A cautionary note, arXiv:1307.5034.

[60] M. Guasoni, J. Garnier, B. Rumpf, D. Sugny, J. Fatome, F. Amrani, G. Millot, and A. Picozzi, Incoherent Fermi-Pasta-Ulam Recurrences and Unconstrained Thermalization Mediated by Strong Phase Correlations, Phys. Rev. X **7**, 011025 (2017).

[61] A. Ramos, L. Fernández-Alcázar, T. Kottos, and B. Shapiro, Optical Phase Transitions in Photonic Networks: A Spin-System Formulation, Phys. Rev. X **10**, 031024 (2020).